Interactions Within the Alcohol Dehydrogenase Zn(II)-Metalloenzyme Active Site: Interplay Between Subvalence, Electron Correlation/ Dispersion, and Charge Transfer/ Induction Effects

BENOÎT DE COURCY,[1,2] JEAN-PIERRE DOGNON,[3] CARINE CLAVAGUÉRA,[4] NOHAD GRESH,[5] JEAN-PHILIP PIQUEMAL[1,2]

[1]*UPMC Univ Paris 06, UMR 7616, Laboratoire de Chimie Théorique, case courrier 137, 4 place Jussieu, F-75005 Paris, France*

[2]*CNRS, UMR 7616, Laboratoire de Chimie Théorique, case courrier 137, 4 place Jussieu, F-75005 Paris, France*

[3]*CEA/Saclay, UMR 3299 CEA/CNRS SIS2M, Laboratoire de chimie de coordination des éléments f, F-91191 Gif-sur-Yvette, France*

[4]*Laboratoire des Mécanismes Réactionnels, Département de Chimie, Ecole Polytechnique, CNRS, 91128 Palaiseau Cedex, France*

[5]*Laboratoire de Pharmacochimie Moléculaire et Cellulaire, U648 INSERM, UFR Biomédicale, Université Paris Descartes, 45, rue des Saints-Pères, 75006 Paris, France*

Received 23 March 2010; accepted 25 March 2010
Published online 17 June 2010 in Wiley Online Library (wileyonlinelibrary.com).
DOI 10.1002/qua.22760

ABSTRACT: Following our preceding works (de Courcy et al. J Chem Theo Comput 2008, 4, 1659; de Courcy, et al. Interdiscip Sci Comput Life Sci 2009, 1, 55), we have studied by quantum chemistry a model of the alcohol dehydrogenase Zn-metalloenzyme (ADH) binding site. Using several interpretative techniques such as

Correspondence to: J.-P. Piquemal; e-mail: jpp@lct.jussieu.fr
Contract grant sponsor: CRIHAN (Rouen, France).
Contract grant number: 2008011.
Contract grant sponsor: GENCI (IDRIS, CINES, France).
Contract grant number: x2010075027 and x2009085107.
Contract grant sponsor: CCRE (Paris, France).

the topological analysis of the electron localization function (ELF) and quantum theory of atoms in molecules combined with energy decomposition analysis schemes, we have analyzed the physical origin of the interactions occurring in this site, which is stabilized by an indirect cation-π interaction. While polarization effects are important for the metal, which is able to adapt its outer-shell density (the so-called subvalence domains) to its ligands, they do not play a key role in the overall interaction of the system that is dominated by dispersion. The ELF analysis shows that only minor charge transfer phenomena are observed between the constitutive fragments of the system. From a methodological standpoint, density functional theory functionals appear unable to handle the system whereas dispersion-corrected methods (DFT-D) perform significantly better, giving reasonable answers as compared with post-Hartree-Fock methods. The stabilization energy brought by the presence of Phe93 to the active binding site of ADH is about -3 kcal/mol. The importance of accounting for basis set superposition error is also emphasized. ©2010 Wiley Periodicals, Inc. Int J Quantum Chem 111: 1213–1221, 2011

Key words: dispersion; DFT; DFT-D; electronic correlation; polarizable force field; metalloenzyme; enzyme; zinc

1. Introduction

Alcohol dehydrogenase (ADH) is a zinc metalloenzyme that catalyzes the reversible oxidation of alcohols into aldehydes or ketones with the concomitant reduction of the coenzyme NAD^+ (Nicotinamide Adenine Dinucleotide) into NADH [1]. In human, it is mainly present in the liver where it initiates the process of the degradation of ethanol. In yeast and many bacteria, it is involved in the opposite reaction as part of fermentation. The mechanism of alcohol oxidation encompasses several steps. It starts with the binding of the NAD^+ coenzyme and of the ethanol substrate to the active site. This is followed by a sequence of proton transfer events. It is initiated by His51 that is deprotonated and then reprotonated by a nicotinamide ribose. This ribose will itself be reprotonated by a Ser48 residue, which in turn, will deprotonate the ethanol substrate. A hydride transfer from the alkoxide ion to NAD^+ then takes place, ultimately leading to the release of acetaldehyde and of NADH. The Zn(II) cation is three-fold coordinated by Cys46, His67, and Cys174 [2]. The ethanol substrate directly binds to the cation and is stacked over the benzene ring of Phe93. These 6 elements, Zn(II), Cys46, His67, Cys174, Phe93, and ethanol, constitute the ADH active site. In the absence of the substrate, a water molecule completes Zn(II) coordination. It is removed by the substrate, because in such systems a five-fold coordinated Zn(II) complex is less stable than the four-fold coordinated complex studied here [3]. The two cysteines are in their deprotonated state [4]. We have analyzed the ADH binding site in two recent contributions [5, 6]. In the last one [6], electron density plasticity was demonstrated using the topology of the electron localization function (ELF) [7, 8]. It was shown that the number of lone pairs borne by ligands in direct interaction with the Zn cation controls the physical nature of the interaction. Thus, it is mainly electrostatic when the core electrons directly face the cation, as is the case of the two S^- atoms, and it is more polarized or covalent when the number of lone pairs facing the cation increases, as is the case for the N lone pair and for the two O lone pairs. As a result, because of the differential polarizing field surrounding it, the Zn(II) cation splits its outer-shell density, toward the ligands, into localization domains (called subvalence basins [9]) whose volumes and populations increase as the nature of the interaction becomes more covalent/polarized. These findings suggest that, polarization is an important energetic contribution in this system. The addition of the benzene ring into the Zn(II) coordination sphere could be intuitively anticipated and stabilize the whole binding site, because of this contribution. However, our previous study [5] showed that, in fact, the polarization energy contributed by the benzene ring was virtually cancelled because of many-body/nonadditivity effects [5]. In this connection, computations using recent quantum chemical topology [10] techniques such as the quantum theory of atom in molecule [(QT)AIM] [11] theory and the ELF through its

evaluation of local electrostatic moments (distributed electrostatic moments based on the ELF Partition or DEMEP analysis [12]), confirmed that the resulting polarization on Zn(II) is represented by its weak dipole moment. The contribution of benzene to complex stabilization actually stems from the dispersion energy, as is the case for typical π-π interactions. Thus physics at play in this active site could be rather complex and requires an adequate treatment of electron correlation, because the dispersion contribution can be central to the stability of the system. An appropriate method should then be sought for. We resort here to several different quantum chemistry methods encompassing several density functional theory (DFT) functionals, DFT-D dispersion corrected functionals, post-Hartree-Fock methods up to coupled cluster and the Sum of interactions between fragments Ab initio computed (SIBFA) polarizable molecular mechanics method [13a] to quantify the role of the dispersion in the stabilization of the active site of ADH as compared with polarization and charge-transfer, both of which sum up into the induction contribution [14]. We will resort again to topological approaches such as ELF and (QT)AIM and of energy decomposition analysis (EDA) schemes, namely the reduced variational space (RVS)[15] and Amsterdam Density Functional (ADF)[16] to analyze the interactions taking place in the ADH active site. The importance of basis set superposition error (BSSE) will also be discussed.

2. Computational Details

2.1. ACTIVE SITE DEFINITION

Figure 1 displays the investigated active site model. It encompasses a Zn(II) cation, 2 cysteinate groups representing the side-chains of deprotonated Cys46 and Cys174 residues, an imidazole moiety representing the side-chain of His67, a benzene ring representing the side-chain of Phe93, and the ethanol substrate. The SIBFA-optimized Zn(II)-ligand distances, and the benzene-ethanol stacking distances were given in Ref [5]. Energy-minimization used the PDB X-ray structure of ADH (code 1adc) [17] as a starting point. It enabled to optimize the location of the missing H atoms and to provide a more realistic coordination distance between Zn(II) and the S^- atom of Cys174, because on account of the resolution, the corresponding PDB

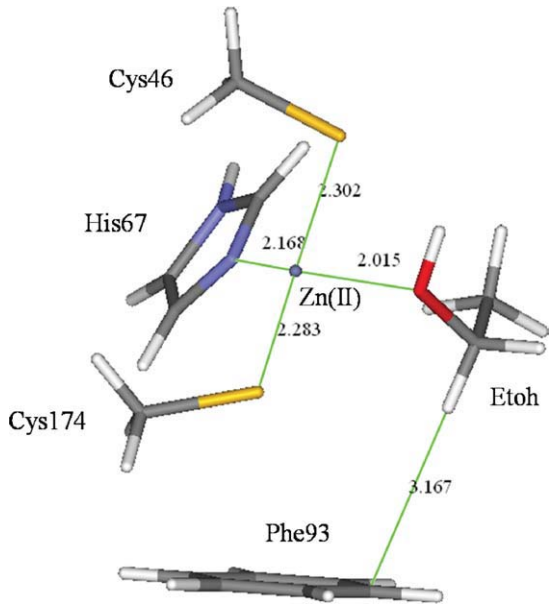

FIGURE 1. Model of the ADH active site. The shortest distance between the ethanol substrate and the benzene ring of Phe93 is of 3.167 Å, and figures the π-interaction. [Color figure can be viewed in the online issue, which is available at wileyonlinelibrary.com.]

distance was too short. Single-point QM and SIBFA calculations were performed on the optimized structures. Two complexes were considered, namely with and without the benzene ring.

2.2. METHODS

RVS [15] EDA analyses at the HF/CEP 4-31G(2d) [18] level of theory, and full MP2 calculations, were done using the GAMESS package [19]. A small core effective potential was used for Zn(II) (18 valence electrons). B3LYP/LACV3P** and lMP2/LACV3P** calculations were realized using the Jaguar software [20], and B3LYP/CEP 4-31G(2d) and MP2/6-311G** using the Gaussian G03 package [21]. The B3LYP functional was chosen as it was shown that it was able to maintain a realistic active site model after optimization [5, 6]. DFT calculations including a dispersion correction (DFT-D) were performed with the ADF program [16] (version 2008.01) using the Perdew-Burke-Ernzerhof (PBE) generalized-gradient approximation exchange correlation functional [22]. Scalar relativistic corrections were included via the ZORA model [23]. TZ2P ZORA basis set (relativistic valence triple-ξ with 2 polarization functions) were used for all atoms. For Zn(II), 20 explicit

electrons were retained. The others were treated by the frozen core approximation. The dispersion correction is implemented in ADF within the S. Grimme framework [24]. MP2 and CC2 interaction energy calculations on SIBFA, DFT-D, and MP2 optimized geometries were performed using the TURBOMOLE 5.10 program package [25] with a triple-zeta TZVPP basis set for all atoms. The CC2 equations are an approximation to the coupled cluster singles and doubles equations, where the single equations are retained in the original form and the doubles equations are truncated to first order in the fluctuation potential [26, 27]. The resolution-of-the-identity approximation was employed for molecular orbital two-particle integrals. The errors made within this approximation are, with optimized auxiliary basis sets, in general negligible as compared with errors due to the one-electron basis set incompleteness. The ADF energy decomposition [28] scheme was used to analyze the bonding properties in the complexes. The bonding energy analysis is performed combining a fragment approach to the molecular structure of chemical systems with the total bonding energy decomposition in electrostatic, Pauli repulsion and orbital mixing terms. A detailed description of the physical significance of these terms has been given by Bickelhaupt and Baerends [28].

2.3. SKETCH ON THE ELF TOPOLOGICAL ANALYSIS

The ELF function [7, 8] can be interpreted as a measure of the Pauli repulsion in the atomic or molecular space and enables access to the probability of finding two same spin electrons: ELF values are restricted between 0 and 1 and can be interpreted as a signature of the electronic pair distribution but, in contrast to pair functions, it can be easily calculated and interpreted. Once computed on a 3D grid from a given ab initio wave function, the ELF function can be partitioned into an intuitive chemical scheme. Indeed, core regions, denoted C(X), can be determined for any atom. This is also the case for valence regions associated to lone pairs, denoted V(X), and for chemical bonds [V(X,Y)]. These ELF regions, the so-called basins (denoted as Ω), match closely the domains of Gillespie's valence shell electron pair repulsion model [29]. It is also important to point out that metal cations exhibit a specific topological signature in the electron localization of their density interacting with ligands according to their "soft" or "hard" character. Indeed, a metal cation can split its outer-shell density (the so-called subvalent domains or basins) according to it capability to form a partly covalent bond involving charge transfer [9].

In addition to a visualization of the ELF isosurfaces, ELF offers the possibility to integrate the population (numbers of electrons) within a basin or to obtain local distributed electrostatic moments such as dipoles and quadrupoles [12]. ELF has been extensively tested on inorganic and bioinorganic systems (see for example [30a–e]). Details about ELF and its applications to systems of biological interest can be found in a recent review paper [30f].

All ELF grids (of size 300*300*300) were generated using the molecular orbitals computed with Gaussian 03 at the B3LYP/6-311++G** level. These ELF computations [and (QT)AIM computations] were performed using a modified TOPMOD package [31].

2.4. POLARIZABLE MOLECULAR MECHANICS COMPUTATIONS

We have used the SIBFA polarizable force field. The intermolecular interaction energy is computed as a sum of 5 separate contributions: penetration corrected multipolar electrostatics (up to quadrupoles), E_{MTP^*} [13b]; anisotropic short-range repulsion, E_{rep} [13c]; polarization, E_{pol}; charge transfer, E_{ct}; and dispersion, E_{disp}. Details on the formulation and calibration of these contributions are given [13a]. The molecular fragments making up the binding site are methanethiolate, imidazole, benzene, and ethanol. They belong to the SIBFA library of fragments. In keeping with our previous studies, the distributed multipoles and polarizabilities are those derived from their HF molecular orbitals computed with the CEP 4-31G(2d) basis set. SIBFA has been extensively tested on Zn(II) complexes and metalloenzymes [5, 13a, d–i].

3. Results and Discussion

3.1. MULLIKEN VS. (QT)AIM VS. ELF: QUANTIFYING CHARGE TRANSFER THROUGH CHARGE ANALYSIS

The induction energy is usually decomposed as polarization and charge-transfer contributions. Previous ELF studies [6] suggested that the Zn(II)

TABLE I

Electron count difference between the electron populations of each fragment constitutive of the ADH active site (the two cysteinates, benzene, Zn(II), ethanol, imidazole) considered as isolated or within the interacting system.

FRAGMENTS	Mulliken	(QT) AIM	ELF
Cysteinate (Cys46)	−0.45	−0.57	−0.07
Imidazole (His67)	0.10	0.13	0.02
Benzene (Phe93)	0.00	0.02	0.00
Cysteinate (Cys174)	−0.34	−0.54	−0.15
Zn^{2+}	0.61	1.01	0.28
Ethanol	0.08	0.03	−0.01

density does delocalize upon the combined action of the ligand electric fields. We reevaluated this result upon comparing (QT)AIM and ELF computations using very dense integration grids to the usual Mulliken population analysis. Table I displays the effective charge transfer in the system computed as the difference between the electron counts of each constitutive fragment of the ADH active site (the two cysteinates, benzene, Zn(II), ethanol, imidazole) considered in isolation on the one hand and complexed on the other hand. Striking differences are observed as the Mulliken and (QT)AIM analysis exhibit strong charge movement whereas the ELF topological analysis tends to show a more limited charge transfer mostly located on the cysteinates, the Zn(II) cation retaining a charge close to two as compared with a charge close to one as derived from the (QT)AIM and Mulliken. This indicates that the observed Zn(II) outer-shell delocalization (ELF subvalence domains [9]) occurs with little actual electron transfer. This demonstrates an almost pure "polarization effect" explaining the fact that no covalent bonding is observed. Indeed at the ELF level, the existence of a V(Zn, X) covalent basin between Zn(II) and a ligand X would constitute the topological sign for electron sharing. The absence of such basins (Fig. 2) suggest that both (QT)AIM and EDA techniques overestimate the amount of charge transfer.

3.2. ENERGY DECOMPOSITION ANALYSIS

Table II reports that the individual energy contributions in the two systems considered, namely in the absence (*a*) and in the presence (*b*) of the Phe93 benzene ring. A third set of data gives the (*b*) − (*a*) energy differences concerning all contributions. It reports the results from three different methodologies. For each set of data, the first column reports the values of the HF/CEP 4-31G(2d) RVS individual energy contributions. The contribution of electronic correlation to the interaction energy ($E_{corr} = E_{MP2} - E_{HF}$) is computed at the MP2/CEP 4-31G(2d) level. It is denoted as δE(MP2). The second column reports the results obtained with the SIBFA procedure, and the two remaining columns report the corresponding energy values obtained through ADF decomposition method at the PBE-D/TZ2P DFT level plus dispersion. The first three columns are single point calculations using the SIBFA geometry, whereas the last column is a single point computation performed after energy-minimization at the PBE-D/TZ2P level. The close match of the SIBFA ΔE interaction energies to ΔE/HF reflects the fact that SIBFA was originally [13a] calibrated at this level of theory. E_1 denotes the sum of the two first-order contributions, namely electrostatic ($E_{Coul.}/E_{MTP}$) and exchange-repulsion ($E_{exch.}/E_{rep.}$). The two QC and the SIBFA values of E_1 are seen to be very close in magnitude. For complex *a*, they differ by 10.6 kcal/mol out of 480, namely a relative error of <2.1%. They differ by 12.3 kcal/mol out of 480 for complex *b*, namely a

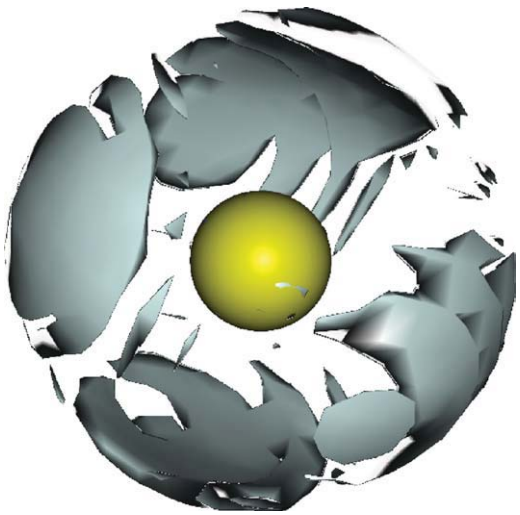

FIGURE 2. Outer-shell delocalization of Zn(II) density (subvalence domains) through its complexation as shown by ELF: the polarized density is not located on the core anymore. This view can be compared with a representation of an uncomplexed Zn(II) that is a perfect sphere. [Color figure can be viewed in the online issue, which is available at wileyonlinelibrary.com.]

TABLE II
Energy decomposition analysis of the interactions within the ADH active site at various levels of theory.

	Complex *a* Without Phe93				Complex *b* With Phe93				Δ = (complex *b* − complex *a*)			
Kcal/mol	HF/MP2	SIBFA	PBE-D	PBE-D (optimized)	HF/MP2	SIBFA	PBE-D	PBE-D (optimized)	HF/MP2	SIBFA	PBE-D	PBE-D (optimized)
$E_{Coul.}/E_{MTP}$	−661.6	−657.9	−719.4	−733.5	−664.4	−662.4	−723.1	−739.5	−2.8	−4.5	−3.7	−6.0
$E_{exch.}/E_{rep}$	177.4	168.9	224.6	225.9	180.2	173.5	226.6	233.7	2.8	4.6	1.9	7.8
E_1	−484.2	−489.0	−494.8	−507.6	−484.2	−488.9	−496.5	−505.8	0.0	0.1	−1.7	1.9
Induction/E_2	−134.0	−135.7	−183.3	−188.0	−133.1	−134.3	−183.1	−190.11	0.9	1.4	0.2	−2.2
ΔE	**−618.2**	**−624.7**	**−678.1**	**−695.6**	**−617.3**	**−623.2**	**−679.6**	**−695.9**	**0.9**	**1.5**	**−1.5**	**−0.3**
δE(MP2)/E_{disp}	−48.4	−65.9	−10.3	−13.7	−57.8	−70.5	−13.3	−20.0	−9.4	−4.6	−3.0	−6.3
ΔE_{tot}	**−666.6**	**−690.6**	**−688.4**	**−709.3**	**−675.1**	**−693.7**	**−692.9**	**−715.9**	**−8.5**	**−3.1**	**−4.5**	**−6.6**

relative error of 2.4%. However, PBE-D values for the induction/E_2 terms, corresponding to the sum of the polarization and charge transfer energetic contributions, are significantly larger than those obtained at the HF and SIBFA levels because of the fact that DFT functionals usually overestimate polarization and charge transfer [32]. This is reflected in Table II by the E2/induction contribution, which appears to be overestimated by ~50 kcal/mol in both complexes, using PBE-D, compared with the corresponding values obtained at the HF and SIBFA levels. It is although worth noticing that the ΔE (before the inclusion of the dispersion term) values computed at the B3LYP/CEP 4-31G(2d) level [5] namely −676.4 and −676.7 for complexes *a* and *b*, respectively, compare closely to the corresponding PBE-D values of −678.1 and −679.6 kcal/mol.

Inclusion of electronic correlation/dispersion terms leads to very different results reflecting the diversity of the methods used to compute them and by summing the individual terms results into consistent outcomes with PBE-D and SIBFA energy values differing by 2.2–0.8 kcal/mol out of 670 corresponding to a relative error of <0.3%. The differences in percentage for the two MP2 values are within the range of 2.9%. Analysis of the differences of the individual energy contributions, Δ(complex *b*–complex *a*) in Table II, given in the third part of the Table, indicates which is the predominant stabilizing contribution due to the benzene ring of Phe93. As already stated [5], no stabilization occurs in the absence of electronic correlation at the MP2 level or dispersion at PMM level. PBE-D calculations confirm this finding. As shown in Table II, using both HF/MP2 and SIBFA, E_1 has a null stabilizing effect following inclusion of this ring. However, DFT-D stabilizes the system by −1.7 kcal/mol, whereas E_2 has a virtually null destabilizing effect. This results into a ΔE stabilization of about −1.5 kcal/mol. The additional contribution of dispersion of −3.0 kcal/mol yields into a −4.5 kcal/mol total DFT-D stabilization energy. The SIBFA optimizations [5] were done upon restraining the position of the first H atom of each ADH side-chain to account for their anchoring in the protein. Although less relevant regarding the actual experimental ADH structure, unrestrained PBE-D energy-minimization identifies the energy contribution which bears most on the stability. At its outcome, the destabilizing electrostatic term (E_1) is found to be compensated by the induction term yielding a stabilizing ΔE of about −0.3 kcal/mol, a

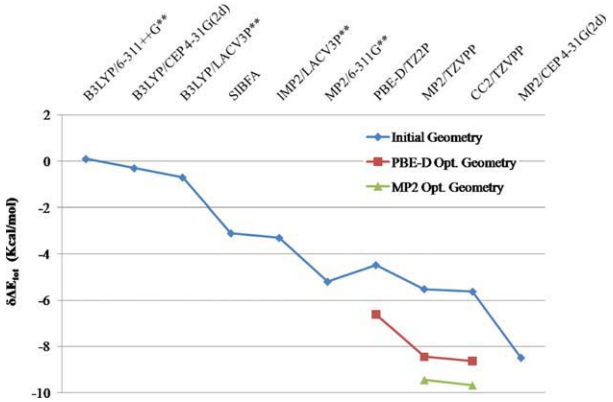

FIGURE 3. Stabilization energy because of Phe93 at various levels of theory. [Color figure can be viewed in the online issue, which is available at wileyonlinelibrary.com.]

value more consistent with the ones obtained with the 2 other methods. Again, dispersion is the major stabilizing contribution, amounting to −6.3 kcal/mol out of −6.6.

Figure 3 reports the $\delta\Delta E_{tot} = \Delta E_{tot}$ (complex *b*) − ΔE_{tot} (complex *a*) energies computed at various levels of theory. Therefore $\delta\Delta E_{tot}$ represents the stabilization energy brought by the benzene ring of Phe93. The blue curve reports the single-point calculations on the SIBFA geometry, the red curve reports the single-point calculations on the geometry obtained after optimization using the PBE-D/TZ2P functional, the green curve is made of single point calculations on the geometry obtained after optimization at the MP2/TZVPP level. This graph shows that DFT without the inclusion of an explicit dispersion term (the two first points) is unable to discriminate between the two complexes, regardless of the basis set ($\delta\Delta E_{tot}$ = 0.1, −0.3, and −0.7 kcal/mol, respectively). The 6 following points are comprised between −3.1 (SIBFA) and −5.6 kcal/mol (CC2/TZVPP), an amplitude of 2.5 kcal/mol representing 0.3% of the lowest value of ΔE_{tot} (−693.7 kcal/mol obtained with SIBFA). The MP2/all atoms (CEP 4-31G(2d) pseudopotentials, known to greatly overestimate the BSSE in cation-π interactions [33], is responsible for the lowest energy of the curve (−8.5 kcal/mol): this will be discussed in the next paragraph. For the two remaining curves, optimization processes have only lowered the energies, displaying a noteworthy parallelism with the curve in blue using the SIBFA geometry.

3.3. ANALYSIS OF THE BSSE EFFECTS

In this study, the $\delta\Delta E_{tot}$ values (Fig. 4) are obtained by subtracting ΔE for two geometries differing solely by the presence of a benzene ring. That way, most of the BSSE effects are removed. This only leaves out the BSSE of the interaction of the benzene with complex *a*. Counterpoise computations have been performed, on the SIBFA geometry, at various levels of theory to estimate its weight within the stabilization energy that was brought by Phe93. For each method, the BSSE in complex *a* was subtracted from that in complex *b* and subsequently removed from $\delta\Delta E_{tot}$. Calculations were done using the B3LYP hybrid functional. Three basis sets of increasing size, CEP 4-31G(2d), LACV3P** and 6-311++G** were considered to evaluate the impact on the magnitude of the BSSE of diffuse functions on the one hand, and of the pseudopotentials on the other hand. BSSE was also calculated using the same methods as reported in Figure 3, except for CC2/TZVPP because the computing cost is unaffordable. The SIBFA and lMP2/LACV3P** results are the same as in Figure 3, as these two methods do not embody BSSE effects by construction. Figure 4 reports the $\delta\Delta E_{tot}$ corrected from the BSSE (red curve) as compared with the uncorrected $\delta\Delta E_{tot}$ (blue curve). Concerning the DFT, as expected the BSSE is significantly reduced upon increasing the size of the basis set, decreasing from 1.7 kcal/mol with CEP 4-31G(2d) to 0.6 kcal/mol with the 6-311++G** one. But in any case, the BSSE, either renders $\delta\Delta E_{tot}$ positive, or increases the positive value of $\delta\Delta E_{tot}$. This could imply that, in contrast with the results obtained with the other methods, the presence of the benzene ring would destabilize the complex rather than stabilizing it. The

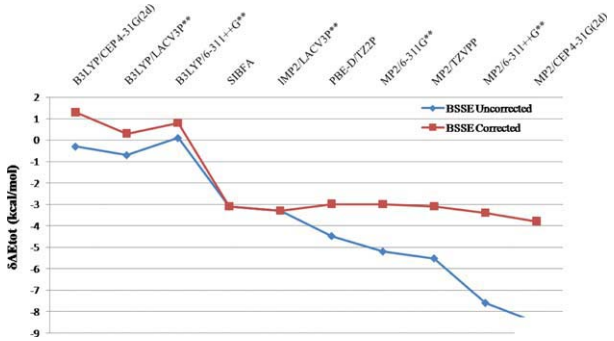

FIGURE 4. Evaluation of BSSE effects upon the initial geometry. [Color figure can be viewed in the online issue, which is available at wileyonlinelibrary.com.]

PBE-D/TZ2P are almost identical to the values obtained with post Hartree-Fock methods. This is not the case with the three previous B3LYP values. This confirms that without the addition of an explicit dispersion term, DFT alone is unable to reproduce such an indirect cation-π interaction. The next five points of the curve show a remarkable consistency, as they have values within a $-3.0/-3.3$ kcal/mol range. BSSE is clearly responsible for the differences in energy shown in the blue curve. It can be noticed that, the two first MP2 calculations overestimate the BSSE, their values representing around 40% of the total $\delta\Delta E_{tot}$. The 10th and last point of the curve shows the greatest BSSE correction, namely 4.7 kcal/mol over a total of -8.5 kcal/mol. This implies that the combined use of MP2 and pseudopotentials on heavy atoms [CEP 4-31G(2d)] necessitates to include the BSSE correction. From these results, it can be deduced that the stabilization energy brought by the presence of Phe93 to the active binding site of ADH is of the order of $-3.0/-3.3$ kcal/mol, as several different calculation methods have given almost the same result. Noteworthy is the performance of the SIBFA PMM procedure, as it is able to reproduce the results obtained with high-level ab initio methods, at a considerably cheaper computing cost.

4. Conclusions

In this report, we have illustrated the different physical origins of the interactions occurring within the active site of the alcohol dehydrogenase Zn-metalloenzyme. The present results confirm that if polarization effects are important for the metal, which is able to adapt its outer-shell density to its ligands, they do not play a key role in the overall interaction of the system that is dominated by dispersion and only subject to minor charge transfer effects. Uncorrected DFT functionals appear to unhandle the system; whereas DFT-D dispersion-corrected methods give reasonable answers compared with post-Hartree-Fock methods. The stabilization energy contributed by the presence of Phe93 to the active binding site of ADH is of the order of $-3.0/-3.3$ kcal/mol. The importance of accounting for the BSSE correction is reemphasized. This study also underlines the good performance of the next-generation SIBFA force-field.

ACKNOWLEDGMENT

The computations reported in this work were performed at the following computer centers: CRIHAN (Rouen, France, on project 2008011), GENCI (IDRIS, CINES, France, on projects x2010075027 and x2009085107) and CCRE (Paris, France).

References

1. Crow, K. E.; Hardman, M. J. In Human Metabolism of Alcohol; Crow, K. E., Batt, R. D., Eds.; CRC Press: Boca Raton, 1989; Vol. 2, p 3.
2. Zaric, S.; Popovic, D. M.; Knapp, E. W. Chem Eur J 2000, 6, 3935.
3. Ryde, U. Int J Quantum Chem 1994, 52, 1229.
4. Nilsson, K.; Ryde, U. J. Inorg Biochem 2004, 98, 1539.
5. de Courcy, B.; Piquemal, J.-P.; Gresh, N. J. Chem Theo Comput 2008, 4, 1659.
6. de Courcy, B; Gresh, N; Piquemal, J.-P. Interdiscip Sci Comput Life Sci 2009, 1, 55.
7. Becke, A. D.; Edgecombe, K. E. J Chem Phys 1990, 92, 5397.
8. Silvi, B.; Savin, A. Nature 1994, 371, 683.
9. de Courcy, B.; Pedersen, L. G.; Parisel, O.; Gresh, N.; Silvi, B.; Pilmé, J.; Piquemal, J.-P. J Chem Theo Comput 2010, 6, 1048.
10. Popelier, P. L. A.; Brémond, E. A. G. Int J Quantum Chem 2009, 109, 2542.
11. (a) Bader, R. F. W. Atoms in Molecules: A Quantum Theory; Oxford University Press: Oxford, 1990; (b) Matta, C. F.; Boyd, R. J. The Quantum Theory of Atoms in Molecules: From Solid State to DNA and Drug Design; Wiley-VCH: Weinheim, 2007; (c) Popelier, P. L. A. Atoms in Molecules: An Introduction; Prentice-Hall: Harlow, U. K., 2000.
12. Pilmé, J.; Piquemal, J.-P. J Comput Chem 2008, 29, 1440.
13. (a) Gresh, N.; Cisneros, G. A.; Darden, T. A.; Piquemal, J.-P. J Chem Theory Comput 2007, 3, 1960; (b) Piquemal, J.-P.; Gresh, N.; Giessner-Prettre, C. J Phys Chem A 2003, 107, 10353; (c) Piquemal, J.-P.; Chevreau, H.; Gresh, N. J Chem Theory Comput 2007, 3, 824; (d) Garmer, D. R.; Gresh, N.; Roques, B. P. Proteins Struct Funct Genet 1998, 31, 42; (e) Tiraboschi, G.; Gresh, N.; Giessner-Prettre, C.; Pedersen, L. G.; Deerfield, W. W. J Comput Chem 2000, 21, 1011; (f) Antony, J.; Piquemal, J.-P.; Gresh, N. J. Comput Chem 2005, 26, 1131; (g) Gresh, N.; Piquemal, J.-P.; Krauss, M. J. Comput Chem 2005, 26, 1113; (h) Roux, C.; Gresh, N.; Perera, L.; Piquemal, J.-P.; Salmon, L. J. Comput Chem 2007, 28, 938; (i) Jenkins, L. M. M.; Hara, T.; Durell, S. R.; Hayashi, R.; Inman, J. K.; Piquemal, J.-P.; Gresh, N.; Appella, E. J Am Chem Soc 2007, 129, 11067.
14. Cisneros, G. A.; Darden, T. A.; Gresh, N.; Reinhardt, P.; Parisel, O.; Pilmé, J.; Piquemal, J.-P. Multi-scale Quantum Models for Biocatalysis: Modern Techniques and Applications, for the Book Series: Challenges and Advances in Computational Chemistry and Physics; York, D. M., Lee, T.-S., Eds.; Springer Verlag, 2009, p 137.

15. Stevens, W. J.; Fink, W. Chem Phys Lett 1987, 139, 15.
16. ADF2008.01, SCM, Theoretical Chemistry, Vrije Universiteit, Amsterdam, The Netherlands, http://www.scm.com
17. Li, H.; Hallows, W. H.; Punzi, J. S.; Pankiewicz, K. W.; Watanabe, K. A.; Goldstein, B. M. Biochemistry 1994, 33, 11734.
18. Stevens, W. J.; Basch, H.; Krauss, M. J Chem Phys 1984, 81, 6026.
19. Schmidt, M. W.; Baldridge, K. K.; Boatz, J. A.; Elbert, S. T.; Gordon, M. S.; Jensen, J. H.; Koseki, S.; Matsunaga, N.; Nguyen, K. A.; Su, S.; Windus, T. L.; Dupuis, M.; Montgomery, J. A., Jr J Comput Chem 1993, 4, 1347.
20. Jaguar 6.5; Schrodinger Inc.: Portland, OR, 2005.
21. Frisch, M. J.; Trucks, G. W.; Schlegel, H. B.; Scuseria, G. E.; Robb, M. A.; Cheeseman, J. R.; Montgomery, J. A., Jr.; Vreven, T.; Kudin, K. N.; Burant, J. C.; Millam, J. M.; Iyengar, S. S.; Tomasi, J.; Barone, V.; Mennucci, B.; Cossi, M.; Scalmani, G.; Rega, N.; Petersson, G. A.; Nakatsuji, H.; Hada, M.; Ehara, M.; Toyota, K.; Fukuda, R.; Hasegawa, J.; Ishida, M.; Nakajima, T.; Honda, Y.; Kitao, O.; Nakai, H.; Klene, M.; Li, X.; Knox, J. E.; Hratchian, H. P.; Cross, J. B.; Bakken, V.; Adamo, C.; Jaramillo, J.; Gomperts, R.; Stratmann, R. E.; Yazyev, O.; Austin, A. J.; Cammi, R.; Pomelli, C.; Ochterski, J. W.; Ayala, P. Y.; Morokuma, K.; Voth, G. A.; Salvador, P.; Dannenberg, J. J.; Zakrzewski, V. G.; Dapprich, S.; Daniels, A. D.; Strain, M. C.; Farkas, O.; Malick, D. K.; Rabuck, A. D.; Raghavachari, K.; Foresman, J. B.; Ortiz, J. V.; Cui, Q.; Baboul, A. G.; Clifford, S.; Cioslowski, J.; Stefanov, B. B.; Liu, G.; Liashenko, A.; Piskorz, P.; Komaromi, I.; Martin, R. L.; Fox, D. J.; Keith, T.; Al-Laham, M. A.; Peng, C. Y.; Nanayakkara, A.; Challacombe, M.; Gill, P. M. W.; Johnson, B.; Chen, W.; Wong, M. W.; Gonzalez, C.; Pople, J. A. Gaussian 03, Revision C. 02; Gaussian Inc.: Wallingford, CT, 2007.
22. Perdew, J. P.; Burke, K.; Ernzerhof, M. Phys Rev Lett 1996, 77, 3865.
23. van Lenthe, E.; Baerends, E. J.; Snijders, J. G. J Chem Phys 1993, 99, 4597.
24. Grimme, S. J Comput Chem 2006, 27, 1787.
25. Ahlrichs, R.; Bär, M.; Häser, M.; Horn, H.; Kölmel, C. Chem Phys Lett 1989, 162, 165 (for current version: see http://www.turbomole.com).
26. Christiansen, O.; Koch, H.; Jørgensen, P. Chem Phys Lett 1995, 243, 409.
27. Hättig, C.; Hellweg, A.; Köhn, A. Phys Chem Chem Phys 2006, 8, 1159.
28. Bickelhaupt, F. M.; Baerends, E. J Rev Comput Chem, Lipkowitz, K. B., Boyd, D. B. Eds.; Wiley-VCH: Indianapolis, USA, 2000, Vol. 15, p 1.
29. Gillespie, R. J.; Robinson, E. A. Chem Soc Rev 2005, 34, 396.
30. (a) Piquemal, J.-P.; Maddaluno, J.; Silvi, B.; Giessner-Prettre, C. New J Chem 2003, 27, 909 (b) Piquemal, J.-P.; Pilmé, J. J Mol Struct: THEOCHEM 2006, 764, 77; (c) de la Lande, A.; Maddaluno, J.; Parisel, O. T. A.; Darden, T.A.; Piquemal, J.-P. Interdiscip Sci Comput Life Sci 2010, 2, 3; (d) Gourlaouen, C.; Piquemal, J.-P.; Parisel, O. J Chem Phys 2006, 124, 174311; (e) van Severen, M.-C.; Piquemal, J.-P.; Parisel, O. Chem Phys Lett 2009, 478, 17; (f) Piquemal, J.-P.; Pilmé, J.; Parisel, O.; Gérard, H.; Fourré, I.; Bergès, J.; Gourlaouen, C.; de la Lande, A.; van Severen, M. C.; Silvi, B. Int J Quantum Chem 2008, 108, 1951.
31. Noury, S.; Krokidis, X.; Fuster, F.; Silvi, B. J Comput Chem 1999, 23, 597.
32. Piquemal, J.-P.; Marquez, A.; Parisel, O.; Giessner-Prettre, C. J Comput Chem 2005, 26, 1052.
33. Paizs, B.; Suhai, S. J Comput Chem 1998, 19, 575.